

Effects of stator splitter blades on aerodynamic performance of a single-stage transonic axial compressor

K. Q. Pham¹, X. T. Le² and C. T. Dinh²

¹ School of Excellent Education, Vietnam Maritime University, 484, Lach Tray Street, Le Chan District, Hai Phong City, 840225, Vietnam

² Aeronautical and Space Engineering Department, Hanoi University of Science and Technology, 1, Dai Co Viet Road, Hai Ba Trung District, Hanoi, 100000, Vietnam

Phone: +842438682525; Fax: +842438684945

ABSTRACT – Splitter blades located between stator blades in a single-stage axial compressor were proposed and investigated in this work to find their effects on aerodynamic performance and operating stability. Aerodynamic performance of the compressor was evaluated using three-dimensional Reynolds-averaged Navier-Stokes equations using the $k-\epsilon$ turbulence model with a scalable wall function. The numerical results for the typical performance parameters without stator splitter blades were validated in comparison with experimental data. The numerical results of a parametric study using four geometric parameters (chord length, coverage angle, height and position) of the stator splitter blades showed that the operational stability of the single-stage axial compressor enhances remarkably using the stator splitter blades. The splitters were effective in suppressing flow separation in the stator domain of the compressor at near-stall condition which affects considerably the aerodynamic performance of the compressor.

ARTICLE HISTORY

Received: 27th Nov 2019

Revised: 10th May 2020

Accepted: 21st June 2020

KEYWORDS

Transonic axial compressor;
stator splitter blades;
RANS analysis;
total pressure ratio;
adiabatic efficiency;
stall margin;
stable range extension

INTRODUCTION

Splitter blades were usually utilized in rotors of centrifugal compressors to improve the performance. The centrifugal impellers with splitter blades were investigated using potential flow models to decrease the loading on the main blades and improve the flow structure at the rotor exit by Bhargava and Gopalakrishnan [1] and Fabri [2]. The results showed that the loading on the main blades and jet/wake effect at the rotor exit were decreased, respectively. The performance of a centrifugal impeller was evaluated experimentally with and without splitter blades by Ogawa and Gopalakrishnan [3]. The results showed that the size and location of the splitter blades were influenced on the overall performance of the centrifugal impeller. Oana et al. [4] suggested that splitter incidence angle affects positively the overall efficiency of an impeller.

The splitter blades were also used in pumps and fans. Kergourlay et al. [5] suggested experimental and numerical studies in the impeller of a hydraulic centrifugal pump (ENSIVAL-MORET MP 250.200.400 pump). The numerical results were matched the experimental data and the pressure fluctuations were decreased at the canal duct. The location of splitter blades was investigated for a centrifugal fan by Madhwesh et al. [6] using CFD code Fluent with a standard $k-\epsilon$. The results showed that the static pressure recovery was increased and the total pressure loss was decreased.

For axial compressors, the splitter blades were introduced in rotor stage in a single-stage transonic axial compressor by Wennerstrom and Frost [7]. The stage total pressure ratio was increased from 3.0 to 3.056. Tzuoo et al. [8] carried out an investigation on the Wennerstrom's rotor [7] using splitter blades based on inviscid and viscous 3-D analysis. The splitter blades in a single-stage axial compressor was presented by Li et al. [9], who simulated and analyzed with 3-D unsteady CFD code. The results showed that splitter blades affected the unsteady static pressure distribution and fluctuation on principle blade, splitter and stator. A new design procedure of a transonic axial compressor rotor with splitter blades was proposed by Drayton [10]. The results showed that the geometry and placement of splitter blades effected on the overall performance of the Wennerstrom's rotor [7].

All the splitter blades in the centrifugal and axial compressor rotors introduced above had the same height with the rotor blades. In the axial compressor with high rotational speed, the splitter blades with small thickness and high span are becoming dangerous in the rotational domain. Until now, no investigation of splitter blades in stator domain of an axial compressor was found in literature. The present work proposes splitter blades in the stator domain of a single-stage transonic axial compressor with a height smaller than 15% of the stator height, to improve the operating stability. A parametric study with four geometric parameters of the stator splitter blades was performed for a single-stage transonic axial compressor, NASA Stage 37 [11] with stator splitter blades using three-dimensional (3-D) Reynolds-averages Navier-Stokes (RANS) equations.

NUMERICAL ANALYSIS

Description of Geometry

The single-stage transonic axial compressor investigated in this work was NASA Stage 37 with 36 blades of Rotor 37 at a rotation speed of 17185.7 rpm (100% of design speed) and 46 blades of Stator 37 [11]. The values of tip clearance for rotor and stator of this single-stage compressor were 0.04 cm and 0.0762 cm, respectively. The total pressure ratio and peak adiabatic efficiency were 2.00 % and 84.00%, respectively, at a mass flow rate of 20.74 kg/s (peak efficiency condition). The mass flow rate at choking and near-stall conditions were 20.93 kg/s and 19.6 kg/s at 100% of design speed and the reference temperature and pressure were 288.15 K and 101,325 Pa, respectively.

The compressor geometry and definition of geometric parameters of the splitter blades are shown in Figure 1. The curvatures of the suction and pressure surfaces of the splitter blades are same as those of the stator blades. The radius of leading edge of the splitter is same as that of the stator leading edge, whereas that of the trailing edge of the splitter blade is equal to 0.05% of the stator blade chord length. The maximum thickness of a splitter blade is equal to 1/3 maximum thickness of a stator blade as illustrated in a small picture in Figure 1. The chord length of splitter blades (C_s), the streamwise distance between the leading edges of splitters and stator blades (L), the height of splitter blades (H) and the angle about the axis of rotation between the pressure surfaces of a splitter and the adjacent stator blades (α), were selected as the parameters of the splitter blades to be tested. Single rotor passage has an angle of 10° ($360^\circ / 36$ blades), and thus the angle (α) was normalized by 10° . The reference design of the splitter blades is presented in Table 1, and the ranges of these parameters for the parametric study were determined as shown in Table 2.

The single-stage transonic axial compressor investigated in this work was NASA Stage 37 with 36 blades of Rotor 37 at a rotation speed of 17185.7 rpm (100% of design speed) and 46 blades of Stator 37 [11]. The values of tip clearance for rotor and stator of this single-stage compressor were 0.04 cm and 0.0762 cm, respectively. The total pressure ratio at peak adiabatic efficiency and peak adiabatic efficiency were 2.00 % and 84.00%, respectively, at a mass flow rate of 20.74 kg/s (peak efficiency condition). The choking mass flow rate is of 20.93 kg/s at 100% of design speed and the reference temperature and pressure were 288.15 K and 101,325 Pa, respectively.

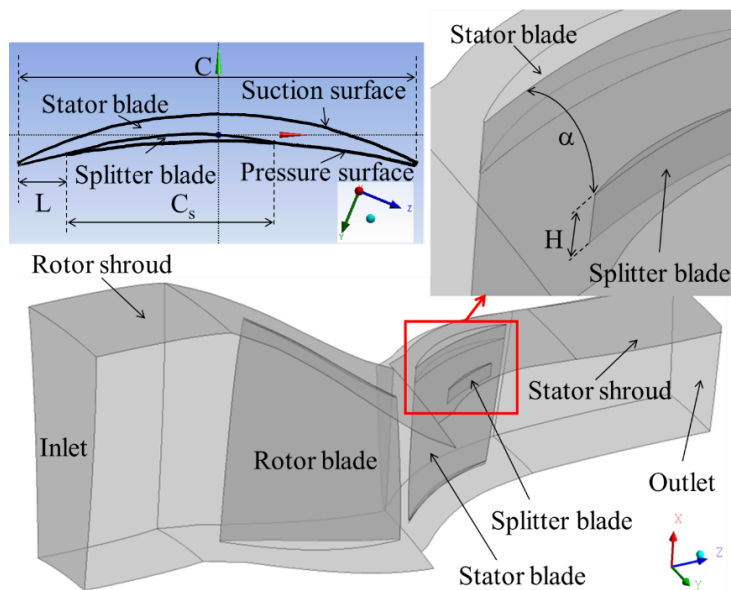


Figure 1. Compressor geometry and geometric parameters of splitter blades

Table 1. Dimensionless parameters of reference design

Variables	C_s/C (%)	L/C (%)	H/S (%)	$\alpha/10^\circ$ (%)
Value	50	0	10	40

Table 2. Ranges of parameters for parametric study

Variables	C_s/C (%)	L/C (%)	H/S (%)	$\alpha/10^\circ$ (%)
Lower	25	0	5	25
Upper	50	50	15	40

Performance Parameters

The compressor aerodynamic performance parameters in this paper are the total pressure ratio (PR), adiabatic efficiency (η), stall margin (SM), and stable range extension (SRE), which are described by Kim et al. [12]–[14] and Dinh et al. [15]–[20] as shown in the following:

$$PR = \frac{P_{t,out}}{P_{t,in}} \quad (1)$$

$$\eta = \frac{\left(\frac{P_{t,out}}{P_{t,in}}\right)^{\frac{\gamma-1}{\gamma}} - 1}{\left(\frac{T_{t,out}}{T_{t,in}}\right) - 1} \quad (2)$$

$$SM = \left(\frac{\dot{m}_{peak}}{\dot{m}_{stall}} \times \frac{PR_{stall}}{PR_{peak}} - 1\right) \times 100\% \quad (3)$$

$$SRE = \left(\frac{(\dot{m}_{max} - \dot{m}_{stall})_{splitter} - (\dot{m}_{max} - \dot{m}_{stall})_{smooth}}{(\dot{m}_{max} - \dot{m}_{stall})_{smooth}}\right) \times 100\% \quad (4)$$

where \dot{m}_{peak} , \dot{m}_{stall} , and \dot{m}_{max} are the mass flow rates at peak efficiency, near-stall, and choke conditions, respectively. PR_{peak} and PR_{stall} are the total pressure ratio at peak efficiency and near-stall conditions, respectively. γ , P_t , and T_t indicate the specific heat ratio, total pressure, and total temperature, respectively.

The stall margin is determined with peak efficiency and near-stall points. The stall margin increases as the pressure rise increases and the mass flow rate decreases at the near-stall point. On the other hand, the stable range extension is determined with choking and near-stall points. And, the stable range extension increases as the mass flow rate at the near-stall point decreases. With a numerical experiment, the authors found that the stator splitter blades reduce the mass flow rate at near-stall point of the single-stage axial compressor, which enhances the operational stability.

Numerical Method

The flow analysis was performed by 3-D RANS analysis, which are averaged from three conservation equations (continuity, momentum and energy conservations) and called Reynolds-averaged Navier-Stokes equations. These averaged equations are presented as follows:

The average continuity equation:

$$\frac{\partial \bar{\rho}}{\partial t} + \frac{\partial}{\partial x_i} (\bar{\rho} \tilde{u}_i) = 0 \quad (5)$$

The average momentum equation:

$$\frac{\partial}{\partial t} (\bar{\rho} \tilde{u}_j) + \frac{\partial}{\partial x_j} (\bar{\rho} \tilde{u}_i \tilde{u}_j) = -\frac{\partial \bar{p}}{\partial x_i} + \frac{\partial}{\partial x_j} (\bar{\tau}_{ij} - \overline{\rho u_i'' u_j''}) \quad (6)$$

The averaged energy equation:

$$\frac{\partial}{\partial t} (\bar{\rho} \tilde{H}) + \frac{\partial}{\partial x_j} (\bar{\rho} \tilde{u}_i \tilde{u}_j \tilde{H} + \overline{\rho u_j'' H''} - k \frac{\partial \bar{T}}{\partial x_j}) = -\frac{\partial \bar{p}}{\partial x_i} + \frac{\partial}{\partial x_j} (\tilde{u}_i \bar{\tau}_{ij} - \overline{u_i'' \tau_{ij}}) \quad (7)$$

Based on the design of NASA Stage 37 with $\dot{m}_{max} = 20.93 \frac{kg}{s}$ and $\dot{m}_{min} = 19.6 \frac{kg}{s}$, the value of Reynolds number for the airflow was from 8×10^5 to 8.6×10^5 , so the airflow in this compressor was totally turbulent. To solve the RANS equations in turbomachinery, most researchers used the k- ϵ and SST turbulence models. Kim et al. [12], [13] presented a comparison between the numerical results using the SST turbulence model and experimental data. The results showed that the numerical results were underlined by a comparison with the experimental data and the relative errors between numerical and experimental results were 3% for total pressure ratio and 3.8% for efficiency, respectively, at the design point. The experimental near stall point was at 0.925 of normalized mass flow rate, while the numerical near stall point was 0.921 of normalized mass flow rate, which was 0.43% of relative error. However, the numerical results using the two-equation k- ϵ turbulence model [15], [16] showed a very good agreement with the experimental data, where the relative errors between numerical and experimental results for total pressure ratio and efficiency were only 1% and 2%, respectively, and the relative error for the near-stall point between numerical simulation and experimental data was only

0.12%. So, the two-equation $k-\varepsilon$ turbulence model with a scalable wall function was selected with y^+ values of the first nodes near the walls in a range from 20 to 100.

ANSYS CFX-19.1 [21] was utilized for analysing the flow analysis. Design-Modeler was used to design the rotor, stator and splitter blades, and Turbo-Grid was employed to generate the meshes. ANSYS CFX-Pre, CFX-Solver, and CFX-Post were used to define boundary conditions, solve the governing equations, and to postprocess the results, respectively.

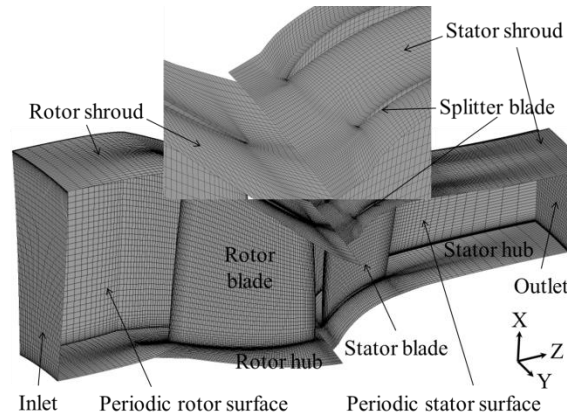


Figure 2. Computational domain and grid structure

The hexahedral elements were used to mesh the computational domain. O-type grids were used near the blade's surface, H/J/C/L-type grids were used in the other regions of the rotor and stator blocks as shown in Figure 2. A grid independency test was performed with three meshes, where Mesh 1, Mesh 2 and Mesh 3 have 336,236, 590,080 and 914,188 nodes, respectively. The working fluid was considered to be an ideal gas. An average static pressure was set at the stator outlet boundary for steady state simulation. A turbulence intensity of 5% was specified at the rotor inlet boundary. The adiabatic smooth wall condition was used for blade surfaces, shroud and hub surfaces of rotor and stator, and also for the splitter surfaces. Periodic conditions were used at the side boundaries of the computational domain. The general grid interface (GGI) method was used for the connection between stator and rotor domains. The frozen rotor method using specified pitch angle ($360^\circ/36 = 10^\circ$ for rotor and $360^\circ/46 = 7.826^\circ$ for stator) was applied for the interface between the rotor outlet and stator inlet. The convergence criteria proposed by Chen et al. [22] were used in this work to determine near-stall point numerically; the inlet mass flow rate variation is less than 0.001 kg/s for 300 steps, the difference between the inlet and outlet mass flow rate is less than 0.3%, and the adiabatic efficiency variation is less than 0.3% per 100 steps.

RESULTS AND DISCUSSION

Grid Independency Test and Validation

Figure 3(a) shows performance curves of the total pressure ratio and adiabatic efficiency using three grid systems having different grid node numbers. And, Figure 3(b) shows the total pressure ratio and adiabatic efficiency at design condition (96.5% of choking mass flow rate). The optimum grid system for the single-stage 37 (smooth casing) is Mesh 2 (590,080 nodes with 340,556 nodes for rotor and 249,524 nodes for stator).

Figure 4 shows the numerical performance curves of the total pressure ratio and adiabatic efficiency for the single-stage transonic axial compressor without splitters compared to the experimental data [11]. The numerical results are qualitatively in good agreements with the experimental data, the adiabatic efficiency is overestimated (about 1.3% at near-stall point), but the total pressure ratio is slightly underestimated (about 0.22% at the peak efficiency). The predicted peak adiabatic efficiency, 83.85% is very close to the measurement, 84.00%. And, the predicted total pressure ratio at peak adiabatic efficiency condition, 2.0045 is slightly higher than the experimental result, 2.000. The predicted near-stall point, 93.85% of the choking mass flow rate is very close to the measurement, 93.65%. The predicted stall margin, 9.95%, is also very close to the measurement, 10.00%.

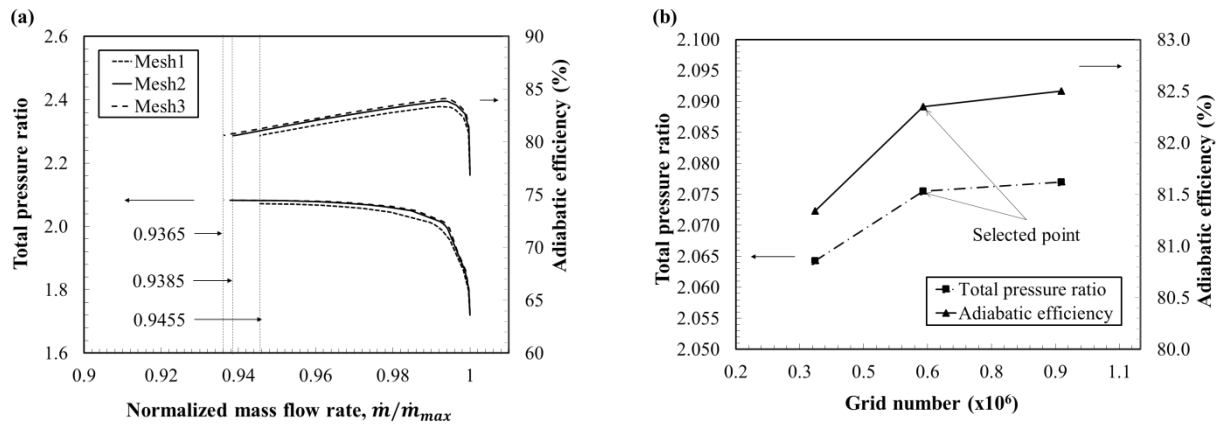


Figure 3. Grid independency tests with smooth casing: (a) performance curves and (b) at design point

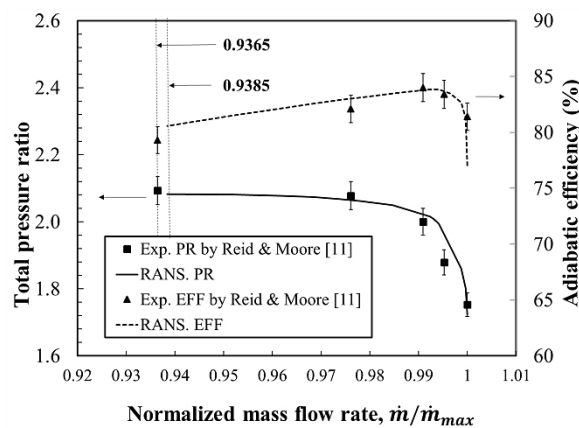


Figure 4. Validation of numerical results with experimental data [11]

Effect of Splitter Design

To examine the effects of the stator splitter design on the aerodynamic performance of a single-stage transonic axial compressor, NASA stage 37, four geometric parameters of the splitter blades were investigated using 3-D Reynolds-averaged Navier–Stokes (RANS) equations. The reference value of the chord length (C_s/C), streamwise distance between the leading edges of splitters and stator blades (L/C), height of splitter blades (H/S) and angle about the axis of rotation between the pressure surfaces of a splitter and the adjacent stator blades ($\alpha/10^\circ$) are 35, 0, 10 and 40, respectively, as shown in Table 1. Figure 5 shows the effect of adding the splitter blades in a single-stage transonic axial compressor as compared to the case with smooth casing. The results show that the near-stall point is largely delayed using the splitter blades (the reference design) compared to the smooth casing from the normalized mass flow rate, 0.9385 (smooth casing) to 0.9336 (reference design). However, the peak adiabatic efficiency of the reference design is slightly decreased from 83.85% (smooth casing) to 83.59% (reference case), and the total pressure ratio at the peak adiabatic efficiency of the reference design (2.000) is almost equivalent to that of the smooth casing (2.0045). The predicted stall margin of the reference design, 10.39%, is higher than that of the smooth casing, 9.95%, and the stable range extension increases from 0.00% (smooth casing) to 8.22% (reference design).

At near-stall condition, low speed zones on 98% span of stator corresponding to Mach number contours of 0.4 are shown in Figure 6, where a low speed zone is pushed away from each stator pressure surface using the splitter blade. When flow separates from the stator blades on the suction surfaces, the splitter contains the flow and keeps it attached, resulting in increasing the stall margin and stable range extension. But, the reference design with the splitter blades (Figure 6(b)) shows also enlargement of the low speed zones corresponded to Mach number contours of 0.2 on the suction surfaces of the splitter blades, which reduces the total pressure ratio and adiabatic efficiency of the axial compressor.

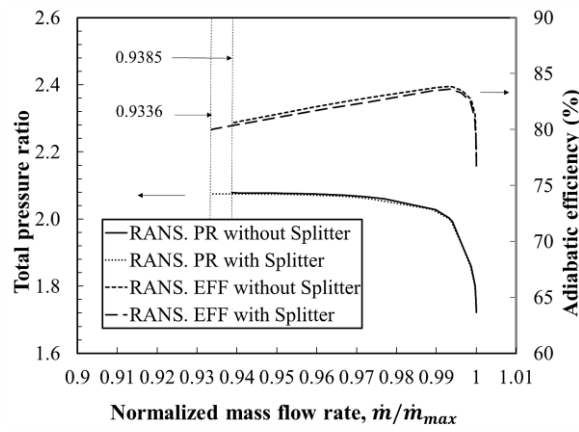


Figure 5. Performance curves of reference design compared with smooth casing

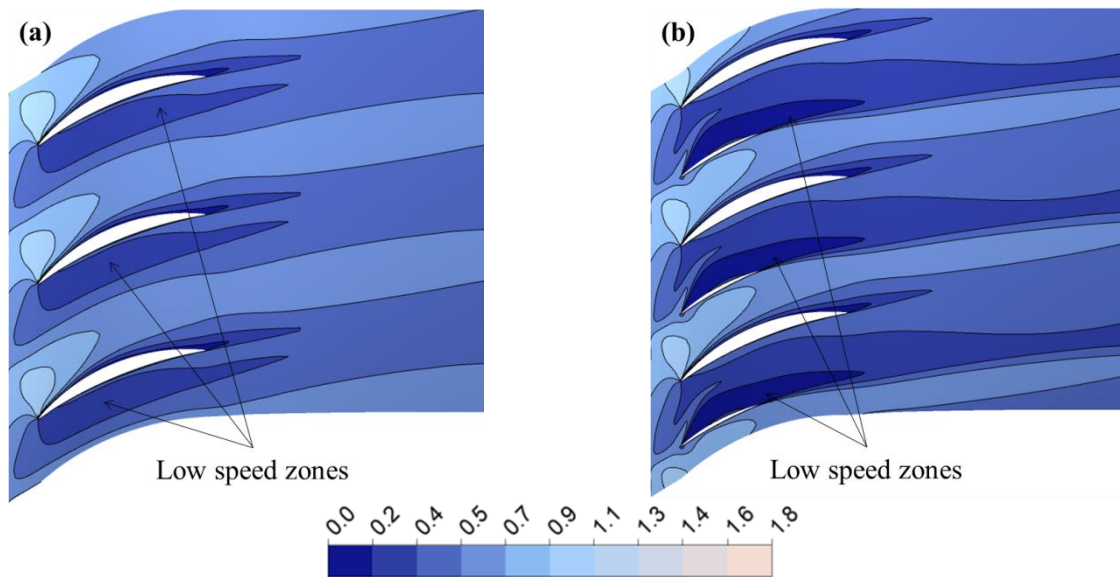
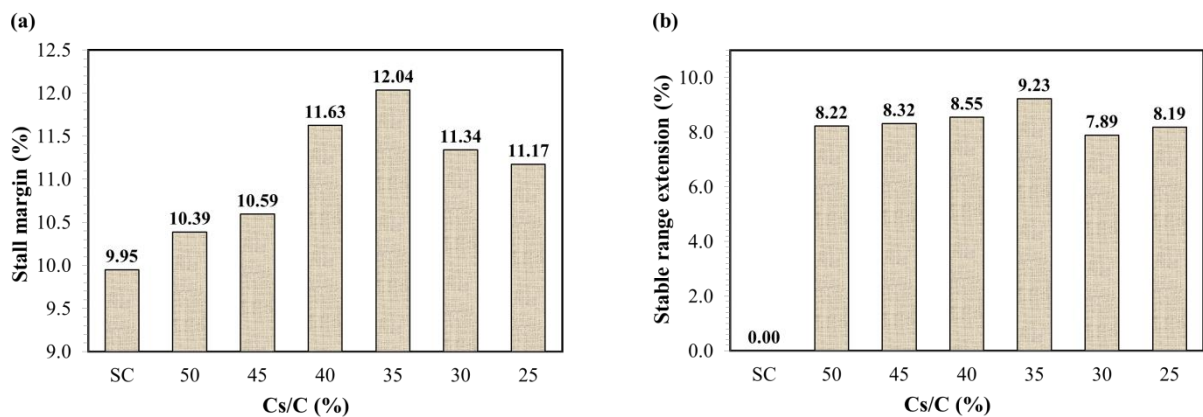


Figure 6. Relative Mach number contours on 98% span in stator domain at near-stall condition: (a) smooth casing and (b) reference case

The aerodynamic performance (total pressure ratio, efficiency, stall margin and stable range extension) of a single-stage transonic axial compressor were investigated for a wide range of splitter geometric parameters (chord length, position, height and angle from the stator pressure surfaces). The splitter parameters are nondimensional with the total 19 models. The results of the parametric study on aerodynamic performance of the single-stage transonic axial compressor using the four parameters of splitter blades (Table 2) are shown in Figures 7-10 to better understand the sensitivity and correlation of each parameter. In the parametric study, the values of the parameters that were not being tested were fixed as the reference values.



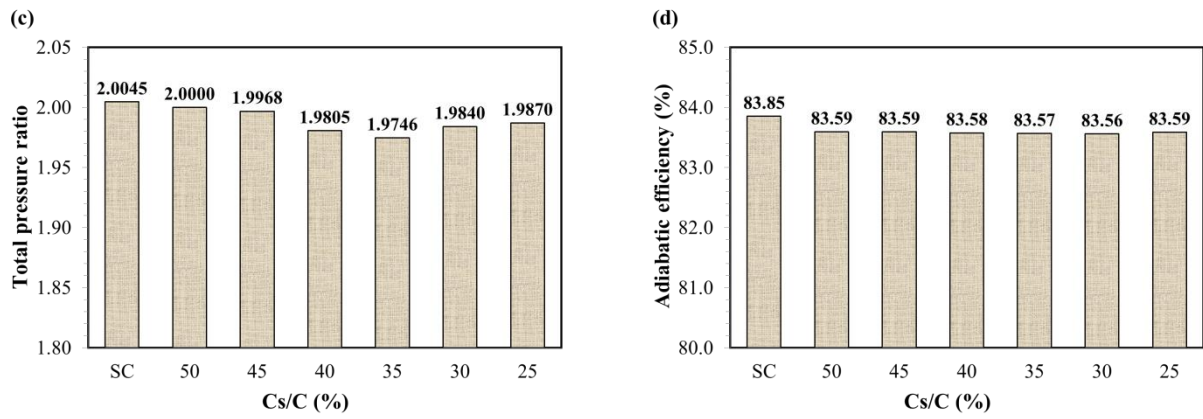


Figure 7. Effect of splitter blade chord length on aerodynamic performances of stage 37: (a) stall margin, (b) stable range extension, (c) total pressure ratio at peak efficiency condition and (d) adiabatic efficiency at peak efficiency condition

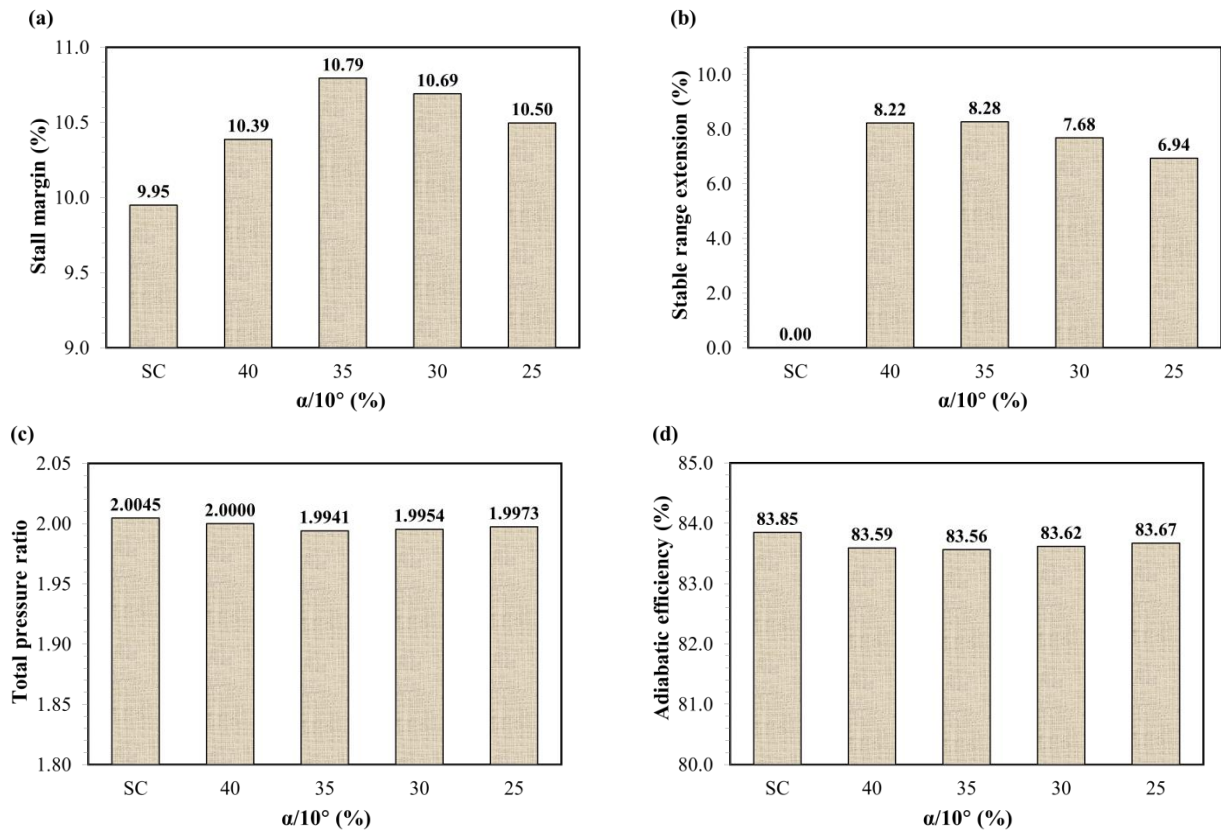


Figure 8. Effect of splitter blade angle on aerodynamic performances of stage 37: (a) stall margin, (b) stable range extension, (c) total pressure ratio at peak efficiency condition and (d) adiabatic efficiency at peak efficiency condition

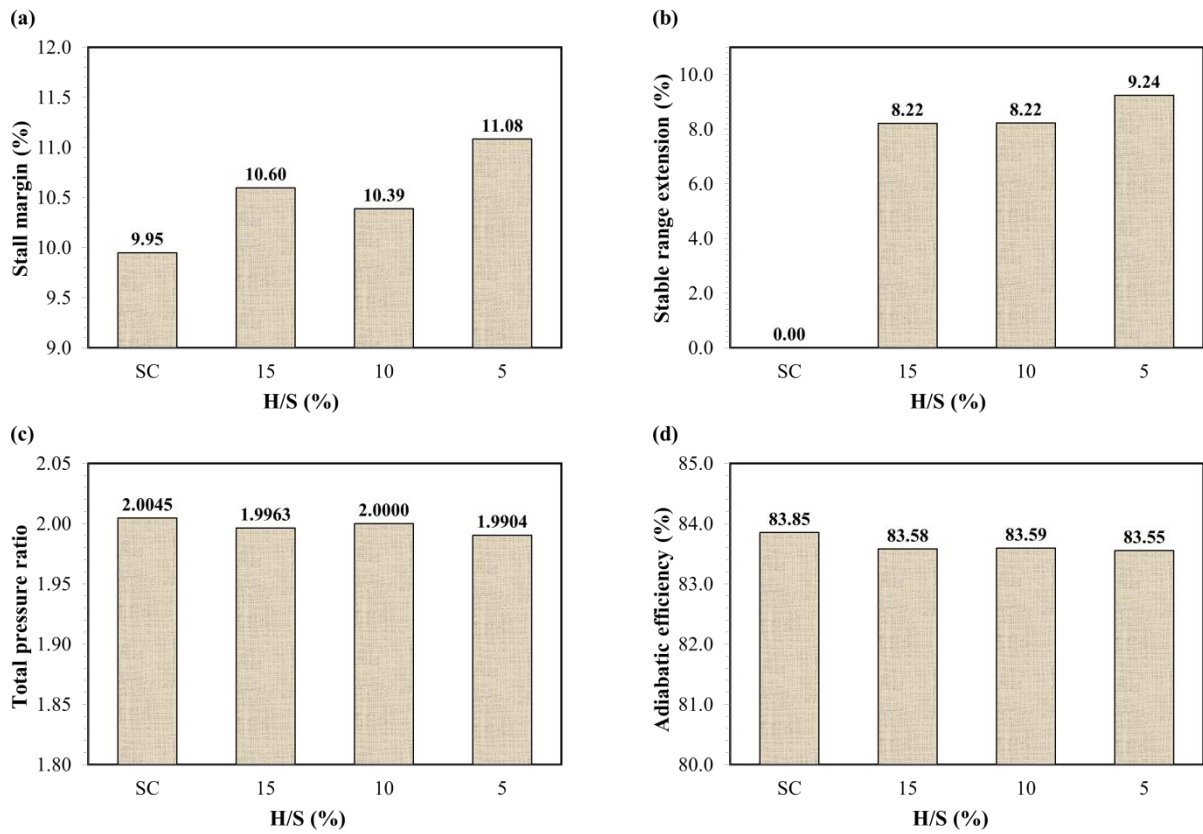


Figure 9. Effect of splitter blade height on aerodynamic performances of stage 37: (a) stall margin, (b) stable range extension, (c) total pressure ratio at peak efficiency condition and (d) adiabatic efficiency at peak efficiency condition

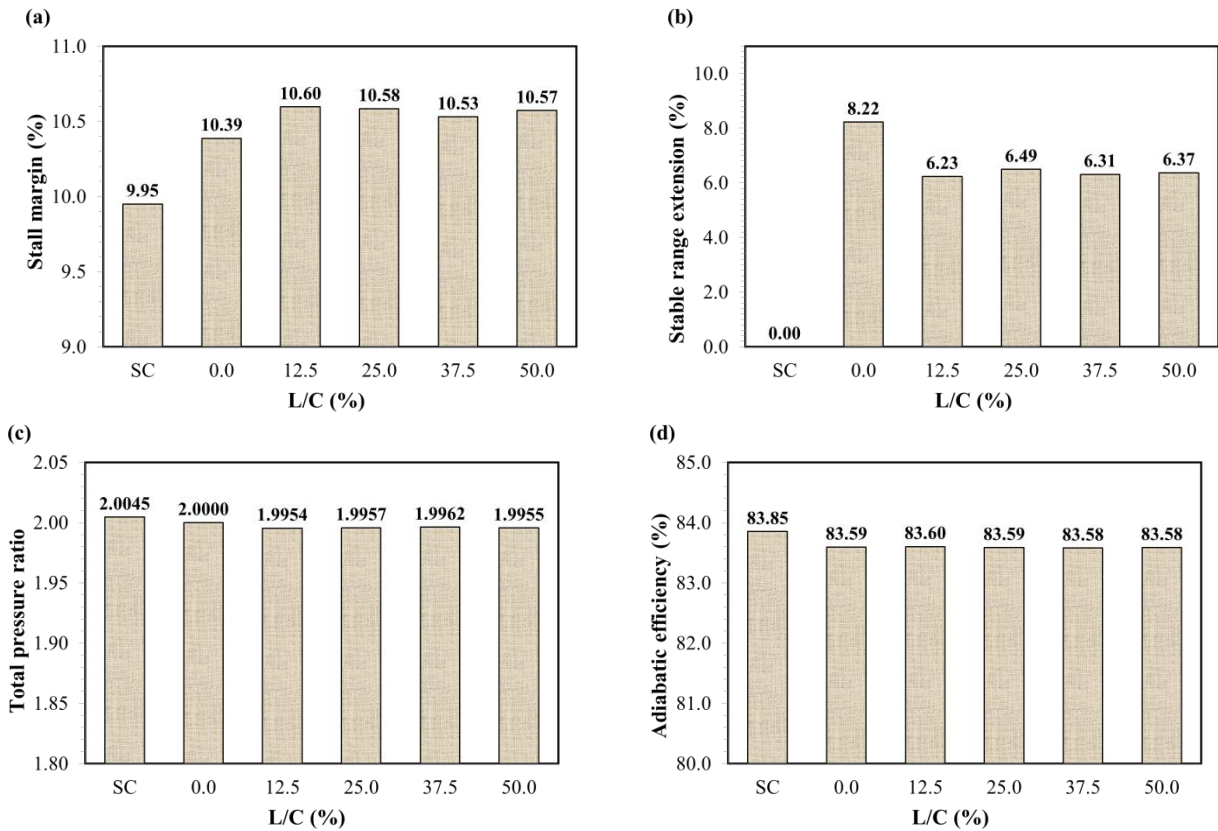


Figure 10. Effect of splitter blade location on aerodynamic performances of stage 37: (a) stall margin, (b) stable range extension, (c) total pressure ratio at peak efficiency condition and (d) adiabatic efficiency at peak efficiency condition

The effect of splitter blade chord length (C_s/C) on aerodynamic performance of the stage 37 is presented in Figure 7. The peak adiabatic efficiencies and the total pressure ratios at peak efficiency with splitter blades are slightly decreased as compared to those of smooth casing; maximum relative reductions of 1.49% for the total pressure ratio and 0.29% for the efficiency as shown in Figures 7(c) and 7(d). However, the stall margins with splitter blades are larger than that of smooth casing. The maximum value of the stall margin is 12.04% at $C_s/C=35\%$, while it is 9.95% for smooth casing as showed in Figure 6(a). The stable range extension using the splitter blades reaches the maximum value of 9.23% at $C_s/C=35\%$ as showed in Figure 7(b). At near-stall condition for $C_s/C=35\%$ in stator domain of a single-stage transonic axial compressor, the low speed zones are highly separated from each stator pressure surface with the splitter blade. That is the main reason of a maximum increase in stall margin and stable range extension as compared to other cases.

Figure 8 illustrates the effect of splitter blade angle (α) on aerodynamic performance of Stage 37. The stall margin and stable range extension are also sensitive to the splitter blade angle. The maximum values are 10.79% for stall margin and 8.28% for stable range extension at $\alpha/10^\circ=35\%$ as shown in Figures 8(a) and 8(b), respectively. This value of splitter blade angle is corresponded to the splitter blade position near the middle of two stator blades. At the value of $\alpha/10^\circ=35\%$, the low speed zones are maximally pushed out from the stator pressure surface as compared to other cases. So, the maximum stall margin and stable range extension are reached at $\alpha/10^\circ=35\%$. Whereas, the peak adiabatic efficiency and the total pressure ratio at peak efficiency condition with splitter blades are slightly reduced as compared to those of smooth casing with a maximum relative reductions of 0.52% for the total pressure ratio and 0.29% for the efficiency as shown in Figures 8(c) and 8(d).

Effect of the height of splitter blades on compressor performance is presented in Figure 9, where the maximum stall margin and stable range extension are 11.08% and 9.24%, respectively, at 5% of stator blade span. It is interesting that the smallest height of the splitter blades shows the best operating stability. However, the peak adiabatic efficiency and total pressure ratio at peak adiabatic efficiency are smallest at 5% of stator blade span as shown in Figures 9(c) and 9(d).

The location of a splitter blade in the flow direction is tested as the last parameter. Figure 10 presents the effect of this parameter on aerodynamic performance of the single-stage transonic axial compressor. The best value of stall margin is 10.60% at $L/C = 12.5\%$ as shown in Figure 10(a), whereas the maximum stable range extension is 8.22% at $L/C = 0\%$ (reference design) as shown in Figure 10(b). The total pressure ratio and efficiency at the peak adiabatic efficiency condition are slightly decreased with a maximum relative reductions of 0.45% and 0.32% for total pressure ratio and efficiency, respectively.

CONCLUSIONS

Splitter blades between stator blades having a height less than 15% stator height were proposed to enhance operating stability of a Single-stage transonic axial compressor, NASA Stage 37. The numerical results using the $k-\epsilon$ turbulence model for total pressure ratio and adiabatic efficiency were validated as compared to experimental data for a smooth casing. The results of parametric study using RANS analysis showed that the splitter blade chord length has most influence on the stall margin, and the maximum stall margin is 12.04% at $C_s/C=35\%$. And, the maximum stable range extension is 9.24% at $H/S = 5\%$. However, the peak adiabatic efficiency and total pressure ratio at peak adiabatic efficiency are slightly reduced with splitter blades from those of smooth casing; maximum relative reductions of 0.224% for the total pressure ratio and 0.26% for the efficiency. Based on the results of this study, the splitter design will be combined with an injection mass flow rate to increase all aerodynamic performance of a single-stage transonic axial compressor in a future work.

ACKNOWLEDGMENTS

The authors would like to acknowledge Vietnam National Foundation for Science and Technology Development under Grant No. 107.03-2018.20.

REFERENCE

- [1] R. K. Bhargava and G. Gopalakrishnan, "Optimising Splitter Vane Locations Using the Method of Singularities," 1978.
- [2] J. Fabri, "Flow Distribution in a Radial Impeller with Splitter Vanes," 1978.
- [3] T. Ogawa and G. Gopalakrishnan, "Use of Splitter Vanes in Centrifugal Compressor Impellers," 1981.
- [4] M. Oana, O. Kawamoto, H. Ohtani and Y. Yamamoto, "Approach to High Performance Transonic Centrifugal Compressor," 2002, doi: 10.2514/6.2002-3536.
- [5] G. Kergourlay, M. Younsi, F. Bakir and R. Rey, "Influence of Splitter Blades on the Flow Field of a Centrifugal Pump: Test-Analysis Comparison," *Int. J. Rotating Mach. Vol. 2007*, vol. 2007, pp. 1–13, 2007, doi: 10.1155/2007/85024.
- [6] N. Madhwesh, K. V. Karanth and N. Y. Sharma, "Impeller Treatment for a Centrifugal Fan using Splitter Vanes – A CFD Approach," in *Proceedings of the World Congress on Engineering 2011*, 2011, pp. 1981–1986.

- [7] A. J. Wennerstrom and G. R. Frost, "Design of a Rotor Incorporating Splitter Vanes for a High Pressure Ratio Supersonic Axial Compressor Stage," *Aerosp. Res. Lab. Rep. ARL 74-0110*, 1974.
- [8] K. L. Tzuoo, S. S. Hingorani and A. K. Sehra, "Design Methodology for Splitted Axial Compressor Rotors," 1990, doi: 10.1115/90-GT-066.
- [9] H. Li, Z. Zou and H. Liu, "Flow Analysis of a Single-stage Axial Compressor with a Splitter Rotor," in *Proceedings of ASME Turbo Expo 2004: Power for Land, Sea and Air*, 2004, pp. 365–373, doi: <https://doi.org/10.1115/GT2004-53265>.
- [10] S. Drayton, "Design, Test, and Evaluation of a Transonic Axial Compressor Rotor with Splitter Blades," Naval Postgraduate School, Monterey, California, USA, 2013.
- [11] L. Reid and R. D. Moore, "Design and Overall Performance of Four Highly Loaded, High-Speed Inlet Stages for an Advanced High-Pressure-Ratio Core Compressor," *NASA Tech. Pap.*, vol. 1337, 1987.
- [12] J. H. Kim, K. J. Choi and K. Y. Kim, "Optimization of a Transonic Axial Compressor considering Interaction of Blade and Casing Treatment to Improve Operating Stability," 2011, doi: 10.1115/GT2011-45404.
- [13] J. H. Kim, K. J. Choi and K. Y. Kim, "Aerodynamic analysis and optimization of a transonic axial compressor with casing grooves to improve operating stability," *Aerosp. Sci. Technol.*, vol. 29, no. 1, pp. 81–91, 2013, doi: 10.1016/j.ast.2013.01.010.
- [14] J. H. Kim, D. W. Kim, and K. Y. Kim, "Aerodynamic optimization of a transonic axial compressor with a casing groove combined with tip injection," *Proc. Inst. Mech. Eng. Part A J. Power Energy*, vol. 227, no. 8, pp. 869–884, 2013, doi: 10.1177/0957650913503311.
- [15] C. T. Dinh and K. Y. Kim, "Effects of Non-axisymmetric Casing Grooves Combined with Airflow Injection on Stability Enhancement of an Axial Compressor," *Int. J. Turbo Jet-Engines*, vol. 36, no. 3, pp. 283–296, 2019, doi: 10.1515/tjj-2016-0077.
- [16] C. T. Dinh, M. W. Heo and K. Y. Kim, "Aerodynamic performance of transonic axial compressor with a casing groove combined with blade tip injection and ejection," *Aerosp. Sci. Technol.*, vol. 46, pp. 176–187, 2015, doi: 10.1016/j.ast.2015.07.006.
- [17] C. T. Dinh, S. B. Ma and K. Y. Kim, "Effects of a Circumferential Feed-Back Channel on Aerodynamic Performance of a Single-Stage Transonic Axial Compressor," 2017, doi: 10.1115/GT201763536.
- [18] C. T. Dinh, S. B. Ma and K. Y. Kim, "Aerodynamic Optimization of a Single-Stage Axial Compressor with Stator Shroud Air Injection," *AIAA J.*, vol. 55, no. 8, pp. 2739–2754, 2017, doi: 10.2514/1.J055909.
- [19] C. T. Dinh, D. Q. Vu and K. Y. Kim, "Effects of Rotor Bleeding Airflow on Aerodynamic and Structural Performances of a Single-stage Transonic Axial Compressor," *Int. J. Aeronaut. Sp. Sci.*, vol. 21, no. 3, pp. 599–611, 2020, doi: 10.1007/s42405-019-00239-5.
- [20] K. Q. Pham, Q. H. Nguyen, T. D. Vuong and C. T. Dinh, "Parametric Study on Aerodynamic Performance of a Single-stage Transonic Axial Compressor with Recirculation-bleeding Channels," *Int. J. Fluid Mach. Syst.*, vol. 13, no. 2, pp. 348–360, 2020, doi: 10.5293/IJFMS.2020.13.2.348.
- [21] ANSYS CFX-19.1., "Theory Guide 2018." ANSYS, Inc., Hanoi, Vietnam, 2018.
- [22] H. Chen, X. D. Huang and S. Fu, "CFD Investigation on Stall Mechanisms and Casing Treatment of a Transonic Compressor," in *42nd AIAA/ASME/SAE/ASEE Joint Propulsion Conference and Exhibit*, 2006, pp. 4789–4798, doi: 10.2514/6.2006-4799.